Acute Exercise Modulates Feature-selective Responses in Human Cortex

Tom Bullock[1], James C. Elliott[1], John T. Serences[2], and Barry Giesbrecht[1]

Abstract

■ An organism's current behavioral state influences ongoing brain activity. Nonhuman mammalian and invertebrate brains exhibit large increases in the gain of feature-selective neural responses in sensory cortex during locomotion, suggesting that the visual system becomes more sensitive when actively exploring the environment. This raises the possibility that human vision is also more sensitive during active movement. To investigate this possibility, we used an inverted encoding model technique to estimate feature-selective neural response profiles from EEG data acquired from participants performing an orientation discrimination task. Participants (n = 18) fixated at the center of a flickering (15 Hz) circular grating presented at one of nine different orientations and monitored for a brief shift in orientation that occurred on every trial. Participants completed the task while seated on a stationary exercise bike at rest and during low- and high-intensity cycling. We found evidence for inverted-U effects; such that the peak of the reconstructed feature-selective tuning profiles was highest during low-intensity exercise compared with those estimated during rest and high-intensity exercise. When modeled, these effects were driven by changes in the gain of the tuning curve and in the profile bandwidth during low-intensity exercise relative to rest. Thus, despite profound differences in visual pathways across species, these data show that sensitivity in human visual cortex is also enhanced during locomotive behavior. Our results reveal the nature of exercise-induced gain on feature-selective coding in human sensory cortex and provide valuable evidence linking the neural mechanisms of behavior state across species. ■

INTRODUCTION

The behavioral state of an organism has dramatic effects on sensory evoked brain responses. Clear demonstrations of these effects come from studies that compare visual cortical activity in awake and anesthetized animals (Sellers, Bennett, Hutt, Williams, & Fröhlich, 2015; Greenberg, Houweling, & Kerr, 2008). Recent neural recordings in awake and behaving animals and invertebrates also reveal robust modulation of neural activity as a function of behavioral state, with evidence that locomotion can influence response gain in visual cortex and subcortical structures (Fu et al., 2014; Ayaz, Saleem, Schölvinck, & Carandini, 2013; Polack, Friedman, & Golshani, 2013; Saleem, Ayaz, Jeffery, Harris, & Carandini, 2013; Keller, Bonhoeffer, & Hübener, 2012; Chiappe, Seelig, Reiser, & Jayaraman, 2010; Maimon, Straw, & Dickinson, 2010; Niell & Stryker, 2010). In the human, not only is cognitive performance influenced by changes in behavioral state that occur with physical activity (Chang, Labban, Gapin, & Etnier, 2012; Lambourne, Audiffren, & Tomporowski, 2010), but a number of studies have used EEG to reveal modulation of brain activity during exercise (Cheron et al., 2016). These investigations indicate that physical activity impacts upon global oscillatory brain activity (Ludyga, Hottenrott, & Gronwald, 2016; Hottenrott, Taubert, & Gronwald, 2013; Fumoto et al., 2010; Bailey, Hall, Folger, & Miller, 2008) as well as patterns of activation that relate to specific stages of cognitive function (Bullock, Cecotti, & Giesbrecht, 2015; De Sanctis, Butler, Malcolm, & Foxe, 2014; Pontifex & Hillman, 2007; Grego et al., 2004).

Although there is evidence that locomotion may act as a gain control mechanism in mouse visual cortex (Wilson & Glickfeld, 2014; Ayaz et al., 2013; Polack et al., 2013; Keller et al., 2012; Niell & Stryker, 2010), the mechanism does not appear consistent across all cell types or at all stages of the visual pathway (Erisken et al., 2014; Saleem et al., 2013). Recent data from mouse auditory cortex also suggest a nonlinear "inverted-U" relationship (Yerkes & Dodson, 1908) between the intensity of physiological arousal and the neuronal response, such that sensory responses were largest and most reliable during moderate arousal when compared with at rest and high arousal (McGinley, David, & McCormick, 2015). Given the vast differences between rodent and primate visual pathways, there is no a priori reason to expect that the human visual system should exhibit the same response to physical activity that has been observed in other species (Laramée & Boire, 2015). However, recent data collected from human participants revealed exercise-induced increases in the scalp-recorded visual evoked P1 ERP component during moderate-intensity exercise when compared with rest and intense exercise (Bullock et al., 2015). These data suggest

[1]University of California, Santa Barbara, [2]University of California, San Diego

that physical activity may induce sensory gain in a manner consistent with the inverted-U model, but they do not inform us of the specific nature of the gain and how this impacts upon feature-selective coding in sensory cortex. Thus, the mechanisms that mediate changes in visual processing that occur with physical activity in human visual cortex are unclear.

Here we tested the effects of physical activity-induced changes in behavioral state on feature-selective, population level neural encoding of visual information in the human brain. To estimate feature-selective response profiles, we applied a computational technique that uses spatially specific patterns of neural activity recorded via noninvasive human neuroimaging techniques. This computational technique, referred to as an inverted encoding model (IEM) has been applied to the BOLD signal measured with fMRI to estimate feature and spatially selective neural response profiles in retinotopically organized visual cortex (Sprague, Saproo, & Serences, 2015; Brouwer & Heeger, 2009, 2011, 2013; Serences & Saproo, 2012). More recently, this method has been used with scalp-recorded EEG to uncover the temporal dynamics of feature-selective processing in the human brain (Garcia, Srinivasan, & Serences, 2013), the focus of spatial attention (Samaha, Sprague, & Pastle, 2016), and the contents of spatial working memory (Foster, Sutterer, Serences, Vogel, & Awh, 2016). We recorded EEG while participants performed an orientation discrimination task during three different behavioral states: at rest and during low- and high-intensity bouts of cycling exercise. We then employed an IEM approach to reconstruct orientation-selective population level response profiles for each condition. Given that previous work with both humans and mice demonstrates inverted-U shaped gain in cortex as a function of exercise intensity (Bullock et al., 2015; McGinley et al., 2015), we predicted that similar U-shaped effects may also occur in the present data. Consistent with our predictions, we found evidence for multiplicative gain during low-intensity exercise when compared with rest and high-intensity exercise. Furthermore, we observed reduced tuning profile bandwidth during low-intensity exercise relative to rest. These data reveal the effects of physical activity on feature-selective coding in human sensory cortex and provide valuable evidence linking the neural mechanisms of behavior state across species.

METHODS

Participants

Eighteen adult volunteers from the University of California, Santa Barbara, community took part in the study, either in exchange for course credit or for financial compensation of $20 per hour. The sample size was determined based on previous studies that have applied an IEM approach to EEG data (Foster et al., 2016; Garcia et al., 2013) as well as investigations of acute exercise effects on cortical activity (e.g., Ludyga et al., 2016; Hottenrott et al., 2013; Bailey et al., 2008). Demographic and physiological data are reported in Table 1. All participants reported having normal vision. All participants completed the Physical Activity Readiness Questionnaire (National Academy of Sports Medicine) to determine their eligibility to participate in aerobic activity. Informed consent was obtained before the start of the experiment. All procedures were approved by the University of California, Santa Barbara, Human Subjects Committee and the U.S. Army Human Research Protection Office.

Table 1. Mean and Standard Error Values for Demographic and Cardiovascular Data

Measure	*Mean Participant Information*
n	18 (9 women)
Age (years)	19.94 (.35)
Height (cm)	172.57 (10.64)
Weight (kg)	69.10 (12.95)
Resting heart rate (BPM)	66 (6.26)
VO_2max (ml/kg/min)	38.52 (9.61)

Visual Stimuli

Visual stimuli consisted of a circular, square wave grating (spatial frequency of two cycles per degree, subtending 7° of visual angle) superimposed with a central fixation point (subtending 0.5° of visual angle). Stimuli were presented on an 19-in. ViewSonic E90f CRT monitor with custom scripts that utilized the Psychophysics Toolbox for MATLAB (Brainard, 1997). Participants viewed the screen at a distance of 110 cm. The eye-tracker was positioned 60 cm from the eye.

Stationary Bike Setup

The stationary bike was a CycleOps 400 Pro Indoor Cycle (Saris Cycling Group, Madison, WI). T2+ Profile Design Aero Bars (Profile Design, Long Beach, CA) were attached to the handlebars and a Logitech Trackball Mouse (Logitech, Newark, CA) was fixed to the end of the bars. The equipment setup is shown in Figure 1A. The addition of the aero bars allowed participants to lean their body weight onto the elbow pads, leaving their hands free to press mouse buttons during the experiment. The bars also helped stabilize the participant and reduce movement of the head and upper body, which is important for reducing the motion artifact during EEG recording. Trainer Road software (Trainer Road, Reno, NV) was used to control the stationary bike, and a CycleOps wireless heart rate monitor was used to monitor heart rate. Our equipment setup is based on the setup described in Pontifex and Hillman (2007), and we have used a similar setup

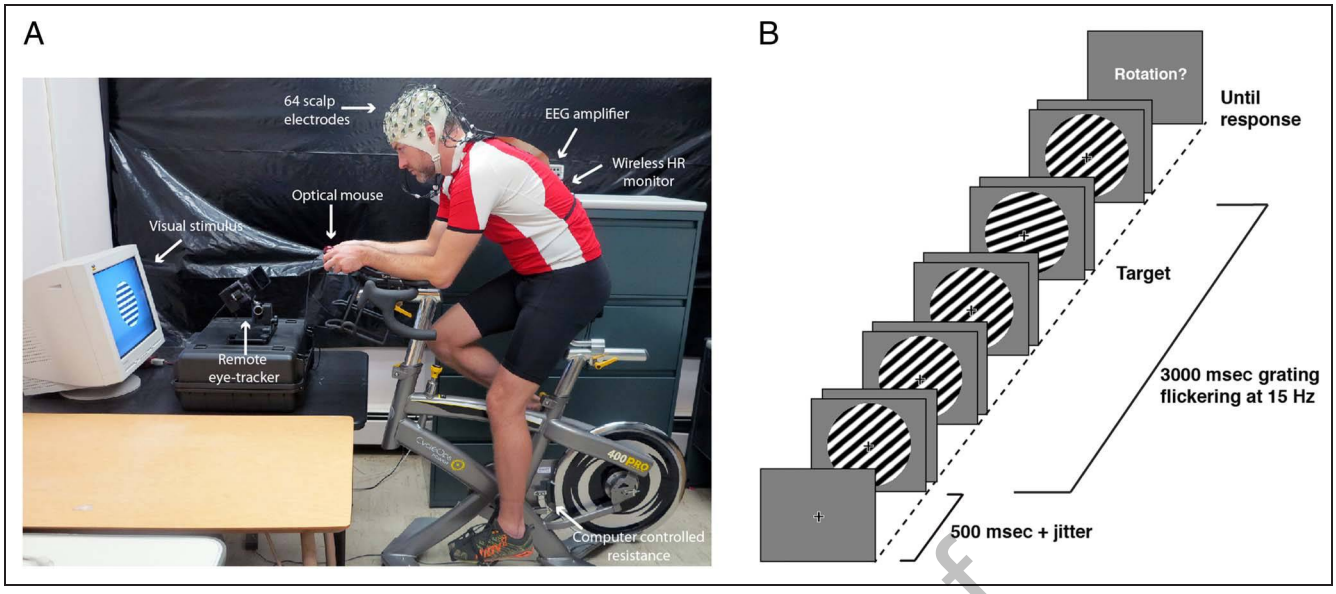

Figure 1. Experimental methods. (A) Equipment setup. (B) Example of rotation offset detection task. Participants fixated at center for the duration of each trial and indicated at the end whether the target rotation offset was clockwise or counterclockwise.

in two previous studies (Bullock et al., 2015; Bullock & Giesbrecht, 2014).

Procedure

Each participant volunteered for two sessions, a pretesting session and the main testing session. The pretesting session was conducted ~1 week before the main session. The pretesting served four key purposes. First, the eye-tracker (Eyelink 1000 Plus, SR Research, Ltd., Mississauga, Ontario, Canada) was tested to ensure that each participant's eye position could be tracked successfully in remote tracking mode. Second, the level of task difficulty for the orientation task was determined for each individual using the method of constant stimuli. Third, each participant's VO_2max was estimated using the Astrand–Rhyming submaximal bike test (Åstrand & Ryhming, 1954). Fourth, seat height and bar position was set to ensure that each participant was comfortable on the stationary bike and able to maintain a steady pedaling cadence at ~50 revolutions per minute (RPM).

At the start of the pretesting session, participants mounted the bike, and were familiarized with the task, and given blocks of practice trials. They then completed a method of constant stimuli procedure consisting of 54 trials of the rotation offset task (see main testing session procedures) presented at six different difficulty levels (ranging between 1° and 8° of rotation offset) in a fully randomized order. This procedure lasted ~40 min and was completed at rest (not pedaling). A Weibull function was then fit to the data to estimate an orientation deviation that resulted in 80% accuracy. Participants then completed the Astrand–Ryming submaximal bike test (Bullock & Giesbrecht, 2014; Åstrand & Ryhming, 1954). During the test, participants were coached to minimize upper body and head movement, and they were instructed to maintain a smooth pedaling cadence of 50 RPM in time to a metronome that sounded at 100 BPM. The values obtained from this procedure provided an estimate of maximal oxygen consumption (VO_2max).

In the main testing session, EEG data were recorded for each participant using a Brain Products ActiCHamp system (Brain Vision LLC, Morrisville, NC) consisting of 64 active electrodes arranged in an actiCAP elastic cap and placed in accordance to the 10–20 System. The TP9 and TP10 electrodes were adhered directly to the right and left mastoids. Data were sampled at 500 Hz and referenced to the average mastoid signal. At the beginning of each investigation, all impedances were <15 kΩ. Participants were then familiarized with the Ratings of Perceived Exertion (RPE) Scale (Borg, 1970). RPE is a subjective rating of the intensity of physical sensations a person experiences during physical activity, including increased heart rate, respiration rate, muscle fatigue, and physical discomfort. Participants reported their RPE throughout the experiment by viewing the Borg scale and reporting a number between 6 (no exertion) and 20 (maximum exertion).

After the EEG electrodes and wireless heart rate monitor were applied, participants then mounted the stationary bike and completed trials of the rotation offset task (Figure 1B). Each trial began with the participant fixating on a centrally presented fixation cross. The trial was initiated by pressing the right mouse button, and after a brief pause (500 msec), a circular grating stimulus appeared and cycled on/off with a blank gray screen at 15 Hz for 3 sec. The 15-Hz flicker was intended to induce a steady-state response that served as the basis for our analysis. The grating was composed of alternating black and

white bars presented at one of nine different orientations, ranging from 0° to 160°. During the trial, the grating rotated either counterclockwise or clockwise for three stimulus cycles, and at the termination of the trial the participant pressed a button to indicate the direction of the rotation offset. The size of the target rotation offset was determined on an individual basis according to each participant's 80% performance threshold calculated using the method of constant stimuli during the pretesting session. The target occurred toward the end of the trial (randomized between 2000 and 3000 msec) on 80% of trials so as to minimize contamination of the orientation-selective response profile. On 20% of trials, the target occurred earlier in the trial (between 133 and 2000 msec) to ensure that participants did not develop a strategy of only attending to the final 1000 msec of the trial; if the participant blinked or moved their eyes more than 1.75° away from the central fixation cross, the trial was immediately terminated and the message "Broken Fixation!" appeared on the screen. Aborted trials were appended to the end of each block, thus ensuring that each participant completed the same number of trials in each exercise condition. Head position was also sampled at 500 Hz throughout each trial by logging the position of a small target sticker placed on the participant's forehead, relative to the position of the eye-tracker.

Each participant performed the orientation task at rest and during low- and high-intensity bouts of cycling exercise. At rest, the participant did not pedal; during low-intensity exercise, the resistance on the bike was fixed at a minimal level (50 W); during high-intensity exercise, the resistance was set at a level that participants self-reported to be "somewhat hard" (12–14 on the RPE Scale; Borg, 1970). Participants were instructed to pedal at 50 RPM to the beat of a metronome to keep cadence consistent across participants and conditions. Exercise condition order was fully counterbalanced across the sample. Participants performed the task until they had completed 36 unbroken trials per block and 10 blocks per condition (broken trials per block [mean ± *SEM*]: rest: 12.9% ± 1.48, low: 18.47% ± 3.50, high: 19.12% ± 3.84).

Each condition took ~40 min to complete, excluding warm-up and cool-down time in the low- and high-intensity exercise conditions. Before the first active condition (either low- or high-intensity exercise, depending on counterbalancing order), participants warmed up for ~5 min while being given further coaching to ensure that they maintained a smooth pedaling cadence to the beat of the metronome and minimized head and body movement. Care was taken to ensure that heart rate returned to within 15 BPM of resting heart rate after the completion of one active condition before starting the next condition. The entire EEG session took ~5 hr.

EEG Data Preprocessing

MATLAB (version 2013b, The MathWorks, Inc., Natick, MA) was used for offline processing of the EEG data, along with the EEGLAB toolbox (Delorme & Makeig, 2004). The continuous data were low-pass filtered at 30 Hz to remove high-frequency muscle movement artifacts (Bullock et al., 2015; De Sanctis et al., 2014; Pontifex & Hillman, 2007) and high pass filtered at 4 Hz to remove low-frequency activity caused by sweating. The data were epoched between −0.5 and 2.5 sec, trials with blinks/broken fixations were removed, and the data were then submitted to a threshold rejection routine, whereby any electrode with a kurtosis distribution exceeding 5 standard deviations from the mean was excluded (mean number of electrodes excluded: rest 3.9 ± .4 electrodes; low 3.5 ± .5 electrodes; high 3.4 ± .4 electrodes) and trials exceeding ±150 μV in remaining channels were excluded (mean number of trials excluded: rest 4.4 ± 2.2; low 10.9 ± 5.3; high 4.3 ± 2.3). Trials with early target onsets (<2000 msec) were excluded, and the remaining trials were cropped to precisely 2 sec (30 complete stimulus presentation cycles at 15 Hz), thus removing any contamination of the neural response by the target rotation onset. The final step of preprocessing involved converting the 2 sec of pretarget data from the included electrodes and each included trial into a single-sided Fourier spectrum using the standard fast Fourier transform function in MATLAB (*fft.m*).

Pattern Classification Analysis

To determine the extent to which the stimulus evoked responses carried information about orientation, a linear discriminant classifier was trained on the estimates of power and phase angle based on the real and imaginary components of the Fourier coefficients at the stimulation frequency (i.e., 15 Hz). Leave-one-out cross-validation was used to train and test the classifier. Classifier performance was measured by converting correct classifications to proportion correct (*n* correct classifications/total classifications) and comparing to chance (1/9 = 0.111). Hypothesis tests were evaluated against an empirical null distribution estimated using resampling (see Hypothesis Testing).

Inverted Encoding Model

We used an IEM to reconstruct orientation-selective tuning profiles based on the spatial distribution of stimulus-evoked activity across the scalp. The goal of the first part of the model is to estimate the extent to which the linear combination of a priori canonical responses (i.e., a basis set) captures the underlying structure in the observed data. The goal of the second part is to determine how much information the response pattern contains about the stimulus features, to the extent that it supports an accurate stimulus reconstruction. This essentially allows the overall shape of the reconstruction to be quantified. The method adopted here was initially used in fMRI studies (Ester, Sprague, & Serences, 2015; Serences & Saproo, 2012; Brouwer & Heeger, 2009, 2011; Naselaris, Kay,

Nishimoto, & Gallant, 2011) and recently applied to scalp-recorded EEG (Foster et al., 2016; Samaha et al., 2016; Garcia et al., 2013). Like decoding (i.e., pattern classification), IEMs involve both training and testing. Here, training was performed using all trials but one, and testing was performed on the single trial left out. More specifically, for a given individual and condition, m represents the number of EEG electrodes in each data set, n_1 represents the number of trials in the training set (~281 trials), and n_2 represents the number of trials in the testing set (1 trial). Let j be the number of hypothetical orientation channels ($C_1, j \times n_1$), composed of half-sinusoidal functions raised to the seventh power as the basis set. In the current study, nine equally spaced orientations were used (i.e., $j = 9$). Raising the functions to the seventh power was intended to approximate the orientation bandwidth of orientation-selective cells in primate visual cortex (Gur & Snodderly, 2007; Ringach, Bredfeldt, Shapley, & Hawken, 2002; Ringach, Shapley, & Hawken, 2002). For each cross-validation step, the data were separated into independent training and testing sets. For each train–test iteration, B_1 ($m \times n_1$) represents the training set and B_2 ($m \times n_2$) the test set. A standard implementation of the general linear model was then used to estimate the weight matrix (W, $m \times j$) using the basis set (C_1). More specifically, using the general linear model

$$B_1 = WC_1 \tag{1}$$

Then, the ordinary least squares estimate of W can be computed as

$$\hat{W} = B_1 C_1^T \left(C_1 C_1^T\right)^{-1} \tag{2}$$

Using the estimated weight matrix ($\hat{W}$, Equation 2) and the test data (B_2), the channel responses C_2 ($j \times n_2$) can be estimated by

$$\hat{C}_2 = \left(\hat{W}^T \hat{W}\right)^{-1} \hat{W}^T B_2 \tag{3}$$

After the $\hat{C}_2$ was solved for each orientation, the channel response function on each trial was then circularly shifted to a common stimulus-centered reference frame, and the centered response functions were averaged. Thus, by convention, the 0° point on the x axis refers to the orientation of the stimulus that evoked the response profile. The final step was then to square the absolute value of the stimulus centered response function to obtain a measure of power (μV^2).

To investigate the source of potential feature-selective modulations, we fit a von Mises distribution to the observed data. Doing so allowed us to estimate tuning profile response bandwidth; an approach that is consistent with measures of orientation selectivity used in both population level human fMRI and single-unit animal studies (e.g., Byers & Serences, 2014; Niell & Stryker, 2008, 2010; Serences, Saproo, Scolari, Ho, & Muftuler, 2009), as well as gain factor and baseline. The channel tuning functions (CTFs) for each participant and exercise condition were independently fit with a von Mises function (Equation 4) with mean (μ), concentration (k), gain (g), and baseline (b) as independent free parameters that reflect distinct attributes of the function. The parameter μ is analogous to the mean in the normal distribution and k is analogous to the inverse of the variance. Thus, k represents tuning bandwidth (a larger k value reflects increased concentration around the mean, hence reduced bandwidth).

$$f(\theta) = g \times e^{k[\cos(\mu - x) - 1]} + b \tag{4}$$

The von Mises function was fit to the data for each participant/condition 150 times using initial seed values for g (0–2), k (0–8), and b (−3 to 3). The μ seed value was fixed at $\pi/2$. Ranges of initial seed values were used to help ensure that the fitting algorithm did not get consistently stuck in a local minimum. The set of parameters for each participant and condition that yielded the lowest root mean squared error across the 150 iterations were then used for subsequent analyses.

Pupil Area, Gaze Position, and Head Motion

Pupil area, gaze position, and head motion data were extracted from the eye-tracking log file. Pupil area was recorded in arbitrary units; eye gaze position in X and Y screen coordinates, which were converted to degrees of visual angle; and head position in arbitrary X (horizontal travel) and Y (vertical travel) units. Pupil area and head motion data were normalized between 0 and 1 using the equation $x_{new} = (x - x_{min})/(x_{max} - x_{min})$. For consistency with the EEG data, trials with early target onsets (<2000 msec) were excluded and remaining trials were cropped to precisely 2 sec. Head motion data from 5 of the 18 participants were not logged, so the remaining 13 participants data were analyzed. To quantify changes in gaze and head motion, a measure of sample dispersion (the distribution of sample cluster around its mean) was calculated for each trial. Sample dispersion S_d is defined according to the equation $S_d = \sqrt{\left(S_x^2 + S_y^2\right)/2}$, where S_x^2 and S_y^2 represent the horizontal and vertical variances of the sampled cluster (Juni, Gureckis, & Maloney, 2015). S_d scores were then averaged across trials to obtain mean gaze dispersion and head motion dispersion scores for each participant and condition.

Hypothesis Testing

Statistical significance of the hypothesis tests was assessed using a nonparametric permutation-based resampling technique to empirically approximate null distributions for the F and t statistics (Foster et al., 2016). This approach has the advantage of being robust to violations of normality. The null distributions were generated according to the

type of data being analyzed. Specifically, for the univariate repeated-measures analyses, we shuffled the condition labels within participants and ran 1000 iterations of the appropriate repeated-measures ANOVA and post hoc t tests, which we then used to generate null distributions of F values and t statistics. For the multivariate decoding and IEM analyses, we shuffled the orientation labels and ran 1000 iterations of the model, reshuffling the labels with every new iteration to create a matrix of 1000 null CTFs for each participant and condition. Where appropriate, we then ran repeated-measures ANOVAs, one-sample t tests, or paired sample t tests on each of the 1000 iterations to generate null distributions of F values and t statistics. Once we had obtained null distributions for each of our data sets, we then tested for reliable difference by calculating the probability of obtaining F and t statistics from each of the null distributions that were greater than the observed F and t statistics. The standard observed F and t statistics for each test are reported in the text, along with the critical p value (labeled p_{null}), which represents the probability of observing a value greater than this in the null distribution. To give a more precise sense of the position of the observed statistic in the null distribution we report the tests as $p_{null} < .05$, $p_{null} < .01$, or $p_{null} < .001$. If a p_{null} value of $>.05$ is reported, then the effect was not considered to be statistically reliable. To provide an indication of effect size, partial eta squared (η^2) is reported for ANOVA results and Cohen's d for all t tests. To test for relationships between variables, we used a bootstrap resampling procedure with 1000 iterations to compute mean correlation coefficients and 95% confidence intervals, whereby confidence intervals overlapping zero indicates a nonsignificant result.

RESULTS

Exercise Physiology and Task Performance

We used several measures to confirm the efficacy of our exercise intensity manipulation. First, we compared the exercise intensity conditions (rest, low, high) in terms of heart rate and pupil area. Heart rate (Figure 2A) significantly increased as a function of exercise ($F(2, 34) = 187.31$, $p_{null} < .001$, $\eta^2 = .92$), such that each stepwise increase in intensity caused a significant increase in heart rate (rest vs. low intensity, $t(17) = 9.85$, $p_{null} < .001$, $d = 1.97$; low vs. high intensity, $t(17) = 9.59$, $p_{null} < .001$, $d = 1.04$). Second, we compared exercise-induced changes in pupil area (Figure 2B). The goal behind analyzing the pupil data was to determine the effects of exercise-induced arousal on raw pupil area, so the data were not baseline-corrected. The data for each participant and condition were collapsed across the 2 sec trial epoch for analysis purposes. Pupil area increased as a function of exercise ($F(1, 17) = 41.09$, $p_{null} < .001$, $\eta^2 = .71$), again with each increase in exercise intensity resulting in a significant increase in pupil area (rest vs. low-intensity, $t(17) = 7.84$, $p_{null} < .001$, $d = 0.53$; low- vs. high-intensity, $t(17) = 2.26$, $p_{null} < .05$, $d = 0.15$). These results are consistent with converging evidence from human and animal studies showing that in addition to variation with ambient light, pupil dilation can also be used to index arousal (McGinley et al., 2015; Erisken et al., 2014; Gilzenrat, Nieuwenhuis, Jepma, & Cohen, 2010; Bradley, Miccoli, Escrig, & Lang, 2008). However, an important consideration is that, because of the dual-task nature of our study, the stepwise increase in physical effort is likely accompanied by an increase in mental effort, and this may also contribute to the increased pupil size (Laeng, Sirois, & Gredeback, 2012).

Third, we compared pedaling power output between the two conditions in which the participants were pedaling and observed that power output was greater during high-intensity (mean ± *SEM*: 88.21 ± 21.5 W) compared with low-intensity exercise (50.23 ± 2.44 W; $t(17) = 7.56$, $p_{null} < .001$, $d = 2.48$). In addition, participants' self-reported exertion was greater during high-intensity (RPE 13.33 ± 0.12) compared with low-intensity (RPE 7.63 ± 0.17) exercise ($t(17) = 27.37$, $p_{null} < .001$, $d = 9.28$). There was a small but significant increase in cadence during low-intensity (53.47 ± 2.66 RPM) compared with high-intensity (51.76 ± 2.21 RPM) exercise ($t(17) = 4.29$, $p_{null} < .01$, $d = 0.69$), likely because of the participants' tendency to increase cadence when pedaling resistance was minimal.

Analysis of the task performance data (Figure 2C) revealed a general impairment of orientation discrimination accuracy during exercise compared with rest ($F(2, 34) = 6.71$, $p_{null} < .01$, $\eta^2 = .28$), such that accuracy was lower during both exercise conditions (low and high intensity)

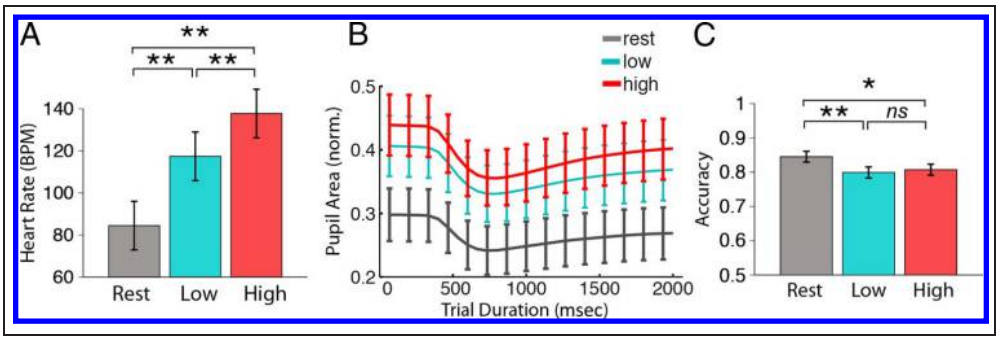

Figure 2. Physiology and behavior. (A) Mean heart rate increased as a function of exercise. (B) Normalized pupil area measured over the first 2000 msec of the trial significantly increased as a function of exercise. (C) Target discrimination accuracy decreased slightly as a function of exercise. *$p_{null} < .05$, **$p_{null} < .001$.

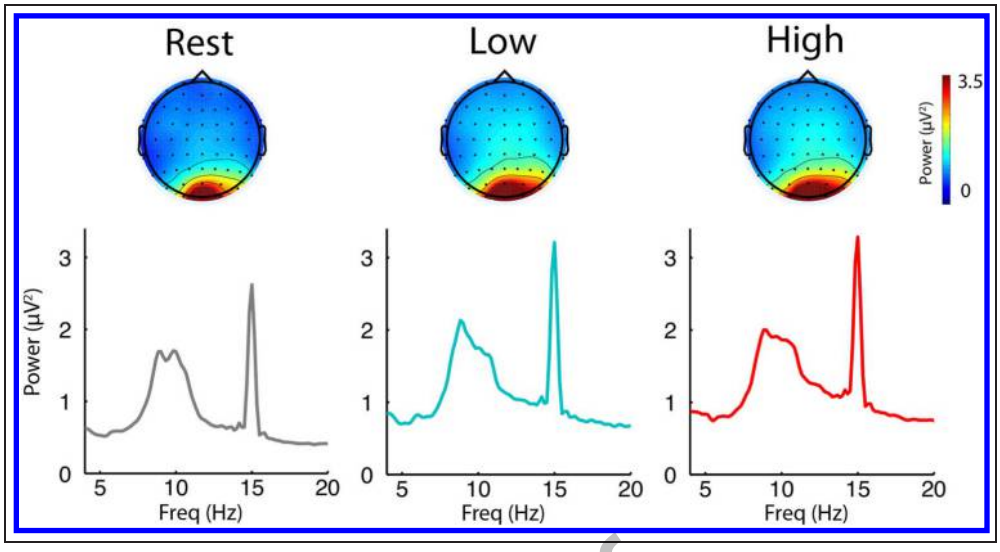

Figure 3. Steady-state responses. We observed robust responses at 15 Hz across occipital and parieto-occipital electrodes (plots represent spectral power averaged over electrodes Oz, O1, O2, POz, PO3, and PO4 and plotted between 4 and 20 Hz for each exercise condition).

compared with rest ($t(17) = 3.36, p_{null} < .001, d = 0.72$; $t(17) = 2.53, p_{null} < .05, d = 0.62$, respectively), but accuracy in the exercise conditions did not differ ($t(17) = -0.78, p_{null} > .05, d = -0.14$).

EEG Power and Pattern Classification

After preprocessing the EEG data, single-trial power between 4 and 30 Hz was estimated using a fast Fourier transform (see Methods). Our stimulus stream cycled on/off with a blank gray screen at 15 Hz and thus evoked a robust spike in power at the 15-Hz stimulation frequency that was focally distributed at the occipital and parieto-occipital electrodes in each of the three exercise conditions (Figure 3). Mean power at 15 Hz was modulated by exercise intensity ($F(2, 34) = 6.48, p_{null} < .01, \eta^2 = .28$), such that power was significantly higher during both exercise conditions (low and high intensity) compared with rest ($t(17) = 2.52, p_{null} < .05, d = 0.19$; $t(17) = 2.93, p_{null} < .05, d = 0.22$, respectively). Power did not differ between exercise conditions ($t(17) = .58, p_{null} > .05, d = 0.02$). Mouse studies that have manipulated behavioral state using locomotion have reported reductions in low frequency local field potential power (<30 Hz) during locomotion when compared with stationary periods (Polack et al., 2013; Niell & Stryker, 2010). We conducted this analysis on our Fourier coefficients measured at occipital and parieto-occipital channels with a frequency resolution of 0.17 Hz and revealed that estimates of power across the lower-frequency bands (theta: 4–8 Hz, alpha: 8–13 Hz, and beta: 16–30 Hz) were modulated by exercise ($F(2, 34) = 30.9, p_{null} < .001, \eta^2 = .65$), with increased power during low- and high-intensity exercise when compared with rest ($t(17) = 6.16, p_{null} < .001, d = 0.55$; $t(17) = 6.70, p_{null} < .001, d = 0.67$) but no difference in power between exercise conditions ($t(17) = 1.46, p_{null} > .05, d = 0.11$). This result contradicts the mouse studies, but is consistent with previous recordings of EEG activity in humans that show increases in alpha, beta and/or theta frequency bands as a function of exercise (Hottenrott et al., 2013; Bailey et al., 2008).

To determine the extent to which the single trial EEG data carried information about stimulus orientation, estimates of power and phase angle were entered into a linear discriminant classifier using a leave-one-trial-out cross-validation procedure (see Methods). Overall classifier accuracy was above chance (chance = 1/9) in all conditions (rest: $t(17) = 6.43, p_{null} < .001, d = 3.03$; low: $t(17) = 6.89, p_{null} < .001, d = 3.25$; high: $t(17) = 5.57, p_{null} < .001, d = 2.63$; Figure 4). Pairwise comparisons of classifier performance indicated that decoding accuracy was higher during rest compared with high-intensity exercise ($t(17) = 2.36, p_{null} < .05, d = 0.54$), but neither rest nor high-intensity exercise were reliably different from low-intensity exercise ($t(17) = -0.04, p_{null} > .05, d = -0.01$; $t(17) = 2.01, p_{null} > .05, d = -0.57$, respectively).

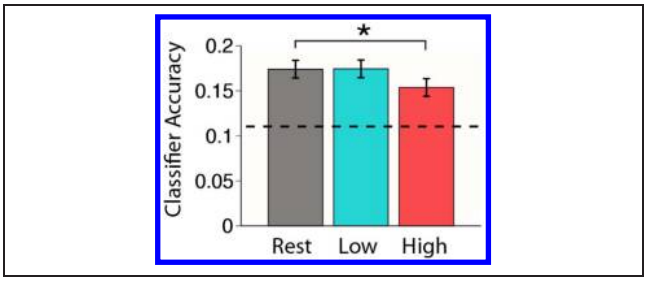

Figure 4. Classification. Classification accuracy in rest, low-intensity, and high-intensity exercise conditions (chance $p = .11$, represented by the dashed line). Data from artifact-free scalp channels were entered into the classifier. *$p_{null} < .05$.

Inverted Encoding Model

To estimate orientation-selective tuning profiles at the population level, we used an IEM modeling technique (e.g., Ester et al., 2015; Foster et al., 2016; Brouwer & Heeger, 2009, 2011, 2013; Garcia et al., 2013; Naselaris et al., 2011). Here we used complex Fourier coefficients estimated at artifact-free electrodes between 0 and 2000 msec on trials in which the target occurred over 2000 msec after trial onset (80% of trials). Doing so ensured that the neural response was not contaminated by target rotation activity. A set of training trials (all trials except for 1) was used to estimate the magnitude of the response at each electrode as a linearly weighted sum of the basis set (an idealized set of orientation tuning functions represented in Figure 5A). These estimated training weights were then used to estimate the relative magnitude of the 15-Hz responses within different subpopulations of neurons (or "channels") that are tuned to different stimulus orientations on the one trial left out from the training set. This process was repeated until all trials served in both training and test sets. The channel responses estimated from the test trials were then averaged and then converted to power by taking the square of the absolute value of the complex numbers. The resulting mean estimated response profiles are termed "channel tuning functions" (CTFs) expressed in terms of power (μV^2).

To first demonstrate the general efficacy of this approach across orientations, we computed CTFs using power at the stimulation frequency (15 Hz) for each of the possible orientations in our stimulus set collapsed across the three exercise conditions. This analysis produced stable tuning curves at each of the nine orientations (Figure 5B). As a second validation step, we estimated CTFs at each frequency from 4 to 30 Hz and then shifted the tuning functions to a common reference, resulting in tuning functions centered on 0° (Garcia et al., 2013). Figure 5C shows the centered CTFs through the tested frequencies (4–30 Hz). There is a clear CTF present at the stimulation frequency of 15 Hz thus confirming that the orientation-selective response information is predominantly carried at the stimulation frequency and not in other bands.

Having demonstrated the efficacy of this approach, the key analyses involved testing whether exercise modulated

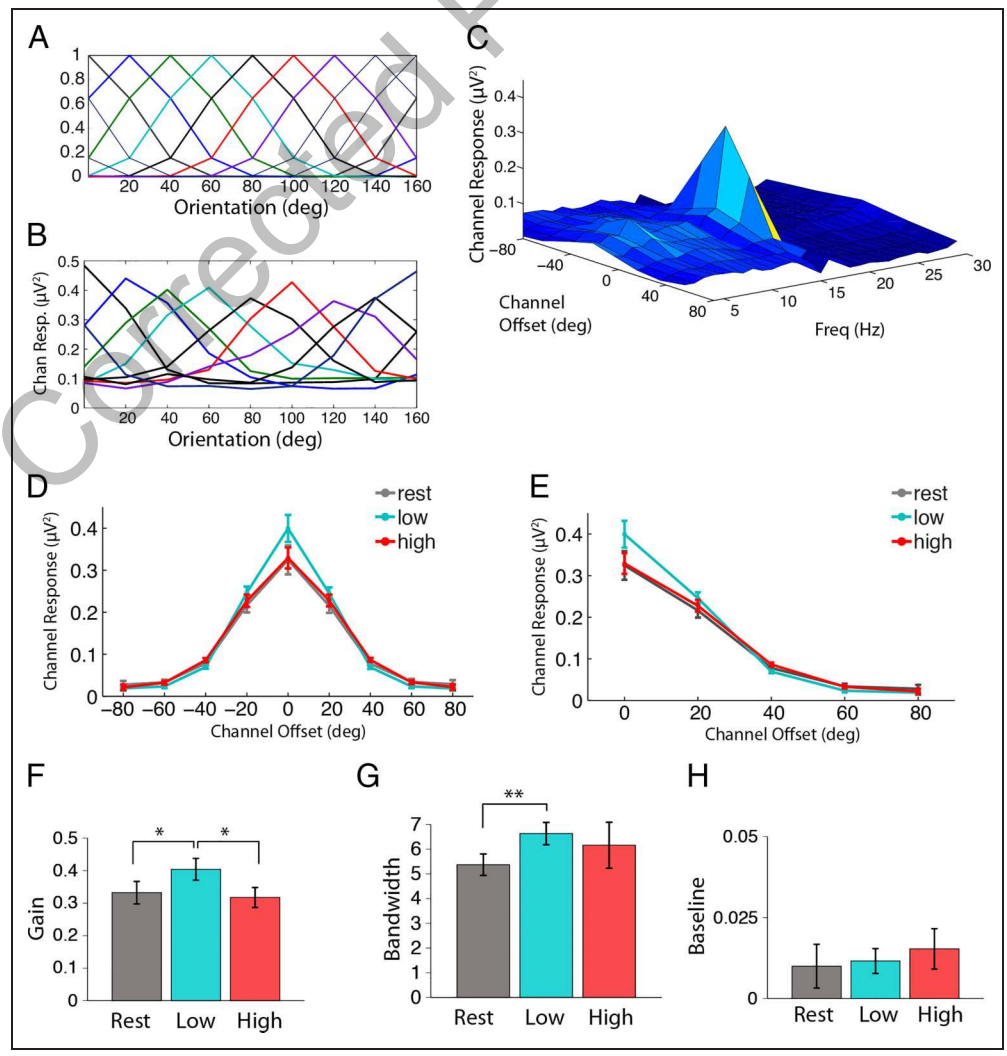

Figure 5. Decoding and encoding. (A) Graded basis set used in IEM. Nine basis functions spanning 0° to 160° in 20° increments were created from half-sinusoidal functions raised to the seventh power. (B) CTFs were derived from the model, using the Fourier coefficients at 15 Hz. This plot depicts CTFs collapsed across exercise conditions before centering. (C) We ran the IEM on all frequencies between 4 and 30 Hz and collapsed across exercise conditions and centered the TFs for ease of plotting. This plot confirms a robust tuning function at 15 Hz. (D) Centered CTFs plotted at 15 Hz for rest, low-intensity, and high-intensity exercise conditions. (E) Centered CTFs were folded from 9 points into 5 points to increase statistical power. Von Mises fitting. Mean gain (F), bandwidth (larger k value reflects reduced tuning profile bandwidth; G), and baseline (H) of the best-fitting von Mises function. Errors bars represent *SEM*. $^{**}p_{null} < .01$, $^{*}p_{null} < .05$.

feature-selective response profiles. To do this, we computed separate CTFs using the Fourier coefficients estimated at 15 Hz for each of the three exercise conditions and then shifted the CTFs to a common center (Figure 5D). To quantify exercise-induced modulation of the shapes of the respective response profiles, we first evaluated changes in CTF amplitude as a function of exercise condition. To increase statistical power, we folded the CTFs from 9 points into 5 points (0°, 20°, 40°, 60°, 80°; Figure 5E) and then entered the folded CTFs into a repeated-measures ANOVA with Exercise intensity (rest, low, high) and Channel offset (0°, 20°, 40°, 60°, 80°) as within-participant factors. This analysis revealed a robust effect of Channel offset ($F(4, 68) = 112.74$, $p_{null} < .001$, $\eta^2 = .87$) and critically a significant Exercise × Channel offset interaction ($F(8, 136) = 3.35$, $p_{null} < .05$, $\eta^2 = .16$). This interaction was driven by increased amplitude of the CTF during low-intensity exercise at the CTF center (0°) and 20° channel offsets ($t(17) = 2.68$, $p_{null} < .01$, $d = 0.52$; $t(17) = 2.39$, $p_{null} < .01$, $d = 0.49$, respectively) and decreased amplitude of the CTF during low-intensity exercise at the 40° and 60° channel offsets ($t(17) = -2.14$, $p_{null} < .05$, $d = -0.46$; $t(17) = -2.17$, $p_{null} < .05$, $d = -0.44$, respectively), relative to the rest condition. The interaction was also driven by increased CTF amplitude during low-intensity exercise relative to high-intensity exercise at the CTF center (0°) and decreased amplitude at 40° ($t(17) = 2.08$, $p_{null} < .05$, $d = 0.56$; $t(17) = -3.04$, $p_{null} < .01$, $d = -0.89$, respectively). CTF amplitude did not differ significantly between rest and high-intensity exercise conditions at any of the channel offsets ($p_{null} > .05$). The selective enhancement around the center of the orientation CTF under low-intensity exercise relative to the other conditions is consistent with the notion that exercise can induce multiplicative gain in feature-selective response profiles.

To further investigate the source of the feature-selective modulations during low-intensity exercise relative to the other conditions, we fit a von Mises distribution to the observed data for each participant and condition (see Methods). One participant was excluded from this analysis because of difficulty in fitting the data in the rest condition. The best fitting parameters for bandwidth, gain, and baseline were entered into paired-samples t tests to compare low-intensity exercise versus rest and low-intensity exercise versus high-intensity exercise. Gain increased during low-intensity exercise relative to both rest and high intensity exercise ($t(16) = 2.28, 2.41$, $p_{null} < .05$, $d = 0.51, .65$, respectively; Figure 5F). Analyses of the bandwidth data revealed an increase in the concentration parameter (k) during low-intensity exercise relative to rest, thus indicating reduced tuning profile bandwidth ($t(16) = 2.53$, $p_{null} < .01$, $d = 0.69$). Bandwidth was not modulated during low-intensity exercise relative to high-intensity exercise ($t(16) = .49$, $p_{null} > .05$, $d = 0.17$; Figure 5G). Baseline was not modulated as a function of low-intensity exercise relative to rest or high-intensity exercise ($t(16) = .26, .53$, $p_{null} > .05$, $d = 0.07, .18$, respectively; Figure 5H).

Control Analyses

Six control analyses were carried out to check the consistency of the main analyses and rule out any alternative explanations.

First, the IEM approach applied here clearly revealed CTFs that exhibited a graded response, such that the peak response is at the center of the function (i.e., the "preferred" orientation) and the response falls off gradually as the angular deviation of the stimulus increases. However, because our basis set used similarly graded functions, it is possible that the graded CTFs observed here were an artifact of the basis set rather than inherent in the EEG data. To rule out this alternative explanation, we reran the analysis replacing the half-wave rectified sinusoid basis set with a set of delta ("stick") functions at each of the nine orientations (Figure 6A). The results of this analysis again revealed graded CTFs modulated by exercise, although the overall amplitude of the response was attenuated relative to the CTFs extracted using the graded basis set (Figure 6B).

Second, after artifact rejection, the number of trials in each of the nine orientations in the training set was not the same (mean trials per set: rest 30.94 ± .16, low 30.71 ± .27, high 30.66 ± .24). We confirmed that there was no systematic bias in the number of training trials per orientation as a function of exercise condition ($F(2, 34) = .94$, $p_{null} > .05$, $\eta^2 = .05$), orientation ($F(8, 136) = .27$, $p_{null} > .05$, $\eta^2 = .02$), or any interaction between the two factors ($F(16, 272) = .57$, $p_{null} > .05$, $\eta^2 = .03$; Figure 6C).

Third, we observed a small but significant increase in pedaling cadence in the low- compared with high-intensity exercise condition. The presence of this difference opens the door to the possibility that the modulations in neural activation we observed were more related to cadence than exercise intensity. If true, then there should be reliable correlations between cadence and our various measures of neural activity (i.e., CTF gain, bandwidth and baseline, power at the stimulation frequency, and global spectral power). Bootstrapped correlations confirmed that there were no significant correlations (Table 2).

Fourth, consistent with studies in the animal literature (McGinley et al., 2015; Erisken et al., 2014), we report a monotonic increase in pupil size as a function of exercise intensity. The magnitude of spherical aberrations increase with pupil size, which is known to degrade the optical quality of the retinal image (Lombardo & Lombardo, 2010), thus raising the possibility that exercise-induced pupil dilation may modulate visuocortical gain. To test this, percent change in pupil area and all neural measures were computed as a function of exercise condition. Bootstrapped correlations confirmed that there were no significant correlations (Table 3), indicating that the exercise-induced changes in neural activity reported here are not confounded by changes in pupil size.

Fifth, our gaze-contingent methodology ensured that any trials where the participant blinked or made eye movements

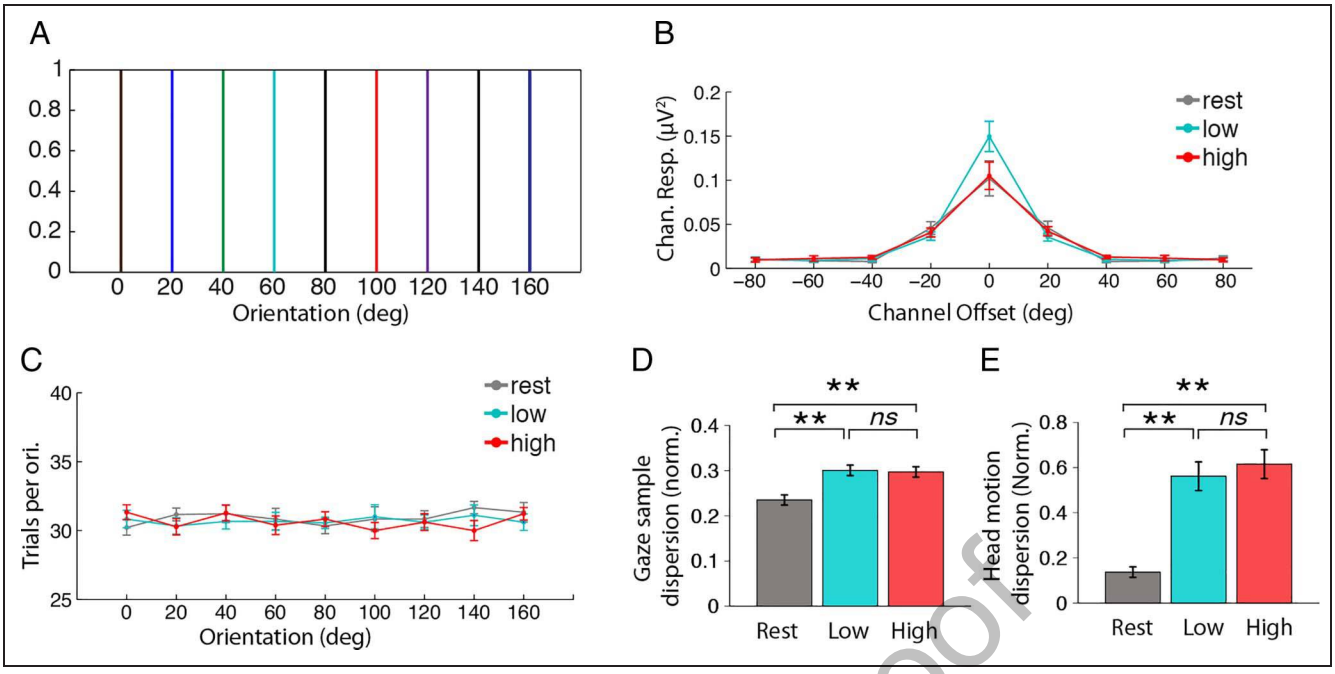

Figure 6. Control analyses. Delta (stick) functions. (A) To rule out the possibility that the CTFs we observed were an artifact of our graded basis set, we reran our IEM replacing the original half-sinusoid basis set with a set of Delta ("stick") functions. (B) The CTFs that we obtained from this analysis revealed graded CTFs with a similar pattern of modulation by exercise as before. Trials per orientation. (C) Plot shows the mean number of trials present for each orientation in the training set following artifact rejection. Gaze dispersion and head motion. (D) Gaze sample dispersion. (E) Head motion sample dispersion. Errors bars represent *SEM*. $^{**}p_{\text{null}} < .001$.

larger than 1.75° from the central fixation cross were rejected online and rerun. However, small changes in gaze dispersion within the acceptable window could be modulated by exercise condition, which may have contributed toward changes in brain activity. If true, there should be reliable correlations between gaze dispersion scores and measures of neural activity (Figure 6D). To test this, we calculated a gaze dispersion score (see Methods). Exercise condition modulated gaze dispersion ($F(2, 34) = 14.22$, $p_{\text{null}} < .001$, $\eta^2 = .46$), with greater dispersion during low- and high-intensity exercise compared with rest ($t(17) = 4.44, 3.67\, p_{\text{null}} < .001, d = 1.37, 1.30$, respectively), but there was no difference between exercise conditions ($t(17) = .42$, $p_{\text{null}} > .05$, $d = 0.07$). To determine if the exercise-induced changes in gaze dispersion tracked with changes in the neural measures, percent change between all exercise conditions (rest vs. low, rest vs. high, low vs. high) was calculated for the gaze dispersion scores and all neural measures, and the percent change values were then correlated (Table 3). There was no relationship between exercise-induced changes in gaze and changes in CTF characteristics, suggesting that the gain and bandwidth modulation effects we observe as a function of exercise cannot be attributed to changes in gaze position within our acceptable window. Similarly, there was no relationship between gaze and the spectral power measures.

Finally, to assess whether our results were attributable to motion artifacts in the EEG data, we quantified head motion using a dispersion metric similar to the gaze position dispersion metric described above. Exercise condition modulated head position dispersion ($F(2, 24) = 54.1$, $p_{\text{null}} < .001$, $\eta^2 = .82$), with greater dispersion during low- and high-intensity exercise compared with rest ($t(12) = 7.82, 9.06$, $p_{\text{null}} < .001$, $d = 2.48, 2.84$), but the exercise conditions were not different ($t(12) = 1.24$, $p_{\text{null}} > .05$, $d = 0.24$) (Figure 6E). As with the gaze position analysis, there were no correlations between head position dispersion and any of the CTF measures (Table 3). There was, however, a relationship between

Table 2. Bootstrapped Correlations Comparing Mean Cadence with Mean Neural Measures during the Low- and High-intensity Exercise Conditions (−95% CI < Mean Rho < +95% CI)

	Low Intensity	*High Intensity*
Cadence		
CTF gain	−.35 < .08 < .46	−.27 < .03 < .40
CTF bandwidth	−.32 < .07 < .31	−.37 < −.01 < .58
CTF baseline	−.58 < −.19 < .34	−.25 < −.10 < .35
Stimulation freq.	−.61 < −.32 < .08	−.54 < −.25 < .22
Global spectral power	−.54 < −.25 < .14	−.63 < −.33 < .06

Table 3. Bootstrapped Correlations Comparing Percent Change in Pupil Area, Gaze, and Head Motion with Percent Change in Neural Measures (−95% CI < Mean Rho < +95% CI)

	%Δ Rest vs. Low	*%Δ Rest vs. High*	*%Δ Low vs. High*
Pupil Area			
CTF gain	−.29 < .03 < .31	−.56 < −.09 < .19	−.38 < −.02 < .39
CTF bandwidth	−.62 < −.25 < .39	−.51 < .04 < .85	−.29 < .23 < .66
CTF baseline	−.43 < −.11 < .41	−.12 < .71 < .99	−.90 < −.28 < .14
Stimulation freq.	−.27 < .28 < .78	−.20 < .31 < .72	−.02 < .35 < .60
Global spectra power	−.75 < .28 < .22	−.67 < −.22 < .26	−.21 < .31 < .58
Gaze Dispersion			
CTF gain	−.22 < .10 < .59	−.29 < .01 < .34	−.72 < −.37 < .13
CTF bandwidth	−.18 < .11 < .45	−.37 < −.04 < .70	−.45 < .06 < .85
CTF baseline	−.47 < −.07 < .28	−.29 < −.07 < .28	−.07 < .20 < .51
Stimulation freq.	−.55 < −.17 < .23	−.51 < −.18 < .30	−.67 < −.41 < .02
Global spectral power	−.66 < −.26 < .10	−.65 < −.34 < .04	−.64 < −.23 < .28
Head Movement Dispersion			
CTF gain	−.57 < −.28 < .41	−.67 < .06 < .53	−.70 < −.01 < .59
CTF bandwidth	−.68 < −.52 < .07	−.77 < −.58 < .17	−.63 < .41 < .10
CTF baseline	−.75 < −.07 < .36	−.87 < −.35 < .35	−.32 < .11 < .75
Stimulation freq.	.21 < .59 < .90*	−.65 < .27 < .65	−.51 < .03 < .73
Global spectral power	.34 < .75 < .95*	−.12 < .51 < .86	−.76 < −.21 < .65

*$p < .05$.

increased head motion and increased global spectral power and power at the stimulation frequency as a function of low-intensity exercise relative to rest.

DISCUSSION

Changes in behavioral state induced by physical activity influence the neural correlates of information processing in humans (Bullock et al., 2015; De Sanctis et al., 2014; Pontifex & Hillman, 2007), rodents (Fu et al., 2014; Ayaz et al., 2013; Saleem et al., 2013; Niell & Stryker, 2010) and invertebrates (Chiappe et al., 2010; Maimon et al., 2010). To investigate the effects of physical activity on feature-selective sensory coding in the human, we applied an IEM approach to scalp recorded EEG acquired at rest and during acute bouts of low- and high-intensity exercise. This approach enabled us to estimate feature-selective response profiles from the spatial distribution of evoked EEG activity across the scalp. Our key finding was that response profiles exhibited an inverted-U pattern as a function of exercise, with response gain during low-intensity exercise relative to both rest and high-intensity exercise, and a reduction in estimated tuning profile bandwidth during low-intensity exercise relative to rest. Critically, the present data go beyond our previous reports of modulation in human sensory cortex as a function of exercise (Bullock et al., 2015) by demonstrating the specific nature of exercise effects on population level feature-selective coding profiles. These findings suggest that evidence for enhanced sensitivity in single-unit non-human mammalian and invertebrate studies may generalize to population level responses in human visual cortex.

Vision is a fundamentally important sensory domain for successful representation of, interaction with, and navigation of the environment; thus, it seems intuitive that physiological arousal induced by acute bouts of activity would induce a high state of gain in visual cortex. The transition to high gain state in visual cortex appears to happen as rapidly as the transition from stationary to running in the mouse (Saleem et al., 2013; Niell & Stryker, 2010), which indicates a close link between visual cortex and motor drive. The present data suggest that behavioral state can also act as a gain modulator in human visual cortex. Furthermore, it is important to note that our IEM technique allows us distinctly different insight to the single unit data, in the sense that we can show effects

of behavioral state on the large-scale populations of neurons that are activated during stimulus representations. The unique advantage of this approach is that it provides a holistic understanding of stimulus encoding, which cannot be obtained by studying single units in isolation (Sprague et al., 2015). Thus, here we extend single-unit observations that behavior state modulates gain to the population level.

Our observation that physiological arousal can have nonlinear effects on neural response gain is also consistent with recent studies of humans and animals (Bullock et al., 2015; McGinley et al., 2015). Gain in the magnitude of the response profile at low- but not high-intensity exercise or at rest is consistent with the inverted-U notion that arousal beyond a certain point is detrimental to performance (Yerkes & Dodson, 1908). We observed these inverted-U effects in a previous study that reported nonspecific ERP evidence for sensory response gain in early visual processing during low-intensity exercise when compared with rest and high-intensity exercise (Bullock et al., 2015). Changes in membrane potential may offer an explanation for these effects. There is evidence that membrane potential in cells in visual cortex becomes more depolarized and less variable during locomotion (Polack et al., 2013), and a recent study in mouse auditory cortex suggests that at medium levels of arousal the membrane potential is low with minimal levels of spontaneous firing, compared with slow oscillations at low arousal and tonic depolarization at high levels of arousal (McGinley et al., 2015).

We acknowledge that there is a mismatch between the inverted-U shaped pattern of exercise effects on CTFs and the drop in task performance as a function of the exercise conditions when compared with rest. There are several key points to consider. First, the decline in task performance as a function of exercise is likely due to the use of the method of constant stimuli to set the orientation task difficulty while participants were at rest (single task) and then requiring them to perform the task at the same difficulty level while concurrently pedaling to the beat of a metronome during the exercise conditions (dual task). Second, the neural activity evoked by the stimulus rotation, which serves as the target-defining feature, is not included in the model. Instead, consistent with the approach used by Garcia, Srinivasan, and Serences (2013), the CTFs are reconstructed from the 2 sec of pretarget activity to prevent interference from the rotation. Furthermore, the reconstructed CTFs are based on neural activity evoked by the steady-state flickering grating at a fixed orientation, whereas the task performance is based on discrimination of rotation away from that orientation, which may require a different type of detector. Hence, it is possible that the increased gain and reduced profile bandwidth during the low-intensity exercise condition may reflect an enhanced detector relative to rest and high-intensity exercise conditions, but the behavioral task is not sensitive to these changes. Third, boosting the signal in local sensory information processing, as appears to be the case in the low-intensity exercise condition, may not necessarily have effects on downstream processing areas and thus may not impact upon task performance (Sprague et al., 2015; Krauzlis, Bollimunta, Arcizet, & Wang, 2014; Zénon & Krauzlis, 2012). Finally, although U-shaped performance curves have been observed as a function of exercise in mice (McGinley et al., 2015), we have also shown mismatch between sensory recordings and behavior in physically active humans in our previous work. In an ERP study, we observed gain modulation in the P1 ERP component during low-intensity exercise, but behavioral performance was only enhanced during high-intensity exercise (Bullock et al., 2015). Several behavioral studies provide indirect evidence for enhancement of sensory processing in humans after a bout of acute physical activity (Davranche & Pichon, 2005; Davranche & Audiffren, 2004); thus, it is entirely possible that exercise effects on sensory processing may enhance human performance in a task that is better suited to measuring this relationship.

Although the IEM results are the primary focus of this discussion, we also acknowledge that the spectral power analyses and classification analysis show different patterns of exercise-induced modulation. The increase in spectral power from 4 to 30 Hz is consistent with previous recordings of EEG activity in humans (Hottenrott et al., 2013; Bailey et al., 2008), and greater spectral power does not imply greater separability of the neural patterns associated with the different orientations, so it is not surprising that the exercise effects on spectral power do not track with the classification or IEM results. Furthermore, it is not unexpected that the pattern classification and IEM results show different patterns of exercise-induced modulation, given the fundamental differences in the nature of these analytical approaches. Classification techniques essentially determine the separability of the classes (i.e., in this case different stimulus orientations) based on observed patterns of neural activation. Other than assuming that there are different classes (e.g., stimulus orientation), classification approaches do not typically make assumptions about the specific structure of the underlying patterns of neural activation to each class. In contrast, encoding models use a set of a priori assumptions about the structure of the feature space (Gur & Snodderly, 2007; Ringach, Bredfeldt, et al., 2002; Ringach, Shapley, et al., 2002) to capture changes in neural codes at the population level, thus enabling stimulus representations to be quantified in terms of native feature space (i.e., gain, bandwidth and baseline) rather than signal space (Sprague et al., 2015; Garcia et al., 2013).

Naturally, there are several limitations to our approach. EEG acquired at the scalp reflects the summed response of dendritic postsynaptic potentials from many different neural populations across the cortex, and thus, our conclusions are limited in the sense that we cannot differentiate between cell types or investigate subcortical function in the human. This is important, as while evidence from the

mouse suggests that most cortical neurons that respond to visual stimulation are excitatory, broad-spiking neurons that show multiplicative gain without changes in feature selectivity as a function of locomotion, there are subsets of cortical neurons and neurons at earlier, subcortical stages of visual processing that show very different patterns of modulation by locomotion (Erisken et al., 2014; Niell & Stryker, 2010). Another important consideration is that, although we do observe large-scale population level modulation of tuning bandwidth as a function of low-intensity exercise relative to rest, this does not imply uniform modulation of tuning profiles across all single units. We also note that the magnitude of the response gain effects observed here in exercising humans are notably smaller than effects observed in locomoting flies and mice (for a summary, see Maimon, 2011), although given that we are comparing scalp-recorded EEG in humans with single-cell action potentials in animals and invertebrates, it is not possible to determine whether these inconsistencies are due to fundamental differences in species or techniques. It is also possible that increased perspiration as a function of exercise might influence the neural data by changing electrode impedances across the conditions; however, if this were the case, we would predict a monotonic change in the fidelity of the model as a function of exercise, not the inverted-U curve observed here. Nevertheless, despite these caveats, the consistencies in overall patterns of locomotion-induced gain represent an important first step in linking behavioral state effects on mouse and human cortex.

In summary, this study used an IEM approach to investigate the influence of behavioral state on estimated response profiles of neurons in human sensory cortex. Our findings indicate that behavioral state can modulate response gain and tuning profile bandwidth in sensory cortex and that the effects of increased physiological arousal may be nonlinear. Thus, despite profound differences in visual pathways across species, these data suggest that evidence for enhanced sensitivity in intracellular non-human mammalian and invertebrate studies may generalize to population level responses in human sensory cortex. This work provides valuable evidence linking the neural mechanisms of behavior state across species and opens the door to further investigations into the influence of physical activity on the human brain.

Acknowledgments

This work was supported by the Institute for Collaborative Biotechnologies through contract W911NF-09-0001 from the U.S. Army Research Office. The content of the information does not necessarily reflect the position or the policy of the Government and no official endorsement should be inferred. We also acknowledge our research assistants, Lena Nalbandian, Greg Gunterson, and Harrison Chung, for their help with data collection.

Reprint requests should be sent to Tom Bullock or Barry Giesbrecht, Department of Psychological and Brain Sciences, University of California, Santa Barbara, CA 93106, or via e-mail: twbullock@googlemail.com, barry.giesbrecht@psych.ucsb.edu.

REFERENCES

Åstrand, P.-O., & Ryhming, I. (1954). A nomogram for calculation of aerobic capacity (physical fitness) from pulse rate during submaximal work. *Journal of Applied Physiology, 7,* 218–221.

Ayaz, A., Saleem, A. B., Schölvinck, M. L., & Carandini, M. (2013). Locomotion controls spatial integration in mouse visual cortex. *Current Biology, 23,* 890–894.

Bailey, S. P., Hall, E. E., Folger, S. E., & Miller, P. C. (2008). Changes in EEG during graded exercise on a recumbent cycle ergometer. *Journal of Sports Science & Medicine, 7,* 505–511.

Borg, G. (1970). Perceived exertion as an indicator of somatic stress. *Scandinavian Journal of Rehabilitation Medicine, 2,* 92–98.

Bradley, M. M., Miccoli, L., Escrig, M. A., & Lang, P. J. (2008). The pupil as a measure of emotional arousal and autonomic activation. *Psychophysiology, 45,* 602–607.

Brainard, D. H. (1997). The Psychophysics Toolbox. *Spatial Vision, 10,* 433–436.

Brouwer, G. J., & Heeger, D. J. (2009). Decoding and reconstructing color from responses in human visual cortex. *Journal of Neuroscience, 29,* 13992–14003.

Brouwer, G. J., & Heeger, D. J. (2011). Cross-orientation suppression in human visual cortex. *Journal of Neurophysiology, 106,* 2108–2119.

Brouwer, G. J., & Heeger, D. J. (2013). Categorical clustering of the neural representation of color. *Journal of Neuroscience, 33,* 15454–15465.

Bullock, T., Cecotti, H., & Giesbrecht, B. (2015). Multiple stages of information processing are modulated during acute bouts of exercise. *Neuroscience, 307,* 138–150.

Bullock, T., & Giesbrecht, B. (2014). Acute exercise and aerobic fitness influence selective attention during visual search. *Frontiers in Psychology, 5,* 1–11.

Byers, A., & Serences, J. T. (2014). Enhanced attentional gain as a mechanism for generalized perceptual learning in human visual cortex. *Journal of Neurophysiology, 112,* 1217–1227.

Chang, Y. K., Labban, J. D., Gapin, J. I., & Etnier, J. L. (2012). The effects of acute exercise on cognitive performance: A meta-analysis. *Brain Research, 1453,* 87–101.

Cheron, G., Petit, G., Cheron, J., Leroy, A., Cebolla, A. M., Cevallos, C., et al. (2016). Brain oscillations in sport: Toward EEG biomakers of performance. *Frontiers in Psychology, 7,* 246.

Chiappe, M. E., Seelig, J. D., Reiser, M. B., & Jayaraman, V. (2010). Walking modulates speed sensitivity in Drosophila motion vision. *Current Biology, 20,* 1470–1475.

Davranche, K., & Audiffren, M. (2004). Facilitating effects of exercise on information processing. *Journal of Sports Sciences, 22,* 419–428.

Davranche, K., & Pichon, A. (2005). Critical flicker frequency threshold increment after an exhausting exercise. *Journal of Sport & Exercise Psychology, 27,* 515–520.

De Sanctis, P., Butler, J. S., Malcolm, B. R., & Foxe, J. J. (2014). Recalibration of inhibitory control systems during walking-related dual-task interference: A Mobile Brain-Body Imaging (MOBI) study. *Neuroimage, 94,* 55–64.

Delorme, A., & Makeig, S. (2004). EEGLAB: An open source toolbox for analysis of single-trial EEG dynamics including independent component analysis. *Journal of Neuroscience Methods, 134,* 9–21.

Erisken, S., Vaiceliunaite, A., Jurjut, O., Fiorini, M., Katzner, S., & Busse, L. (2014). Effects of locomotion extend throughout the mouse early visual system. *Current Biology, 24,* 2899–2907.

Ester, E. F., Sprague, T. C., & Serences, J. T. (2015). Parietal and frontal cortex encode stimulus-specific mnemonic representations during visual working memory. *Neuron, 87,* 893–905.
Foster, J. J., Sutterer, D. W., Serences, J. T., Vogel, E. K., & Awh, E. (2016). The topography of alpha-band activity tracks the content of spatial working memory. *Journal of Neurophysiology, 115,* 168–177.
Fu, Y., Tucciarone, J. M., Espinosa, J. S., Sheng, N., Darcy, D. P., Nicoll, R. A., et al. (2014). A cortical circuit for gain control by behavioral state. *Cell, 156,* 1139–1152.
Fumoto, M., Oshima, T., Kamiya, K., Kikuchi, H., Seki, Y., Nakatani, Y., et al. (2010). Ventral prefrontal cortex and serotonergic system activation during pedaling exercise induces negative mood improvement and increased alpha band in EEG. *Behavioural Brain Research, 213,* 1–9.
Garcia, J. O., Srinivasan, R., & Serences, J. T. (2013). Near-real-time feature-selective modulations in human cortex. *Current Biology, 23,* 515–522.
Gilzenrat, M. S., Nieuwenhuis, S., Jepma, M., & Cohen, J. D. (2010). Pupil diameter tracks changes in control state predicted by the adaptive gain theory of locus coeruleus function. *Cognitive, Affective, & Behavioral Neuroscience, 10,* 252–269.
Greenberg, D. S., Houweling, A. R., & Kerr, J. N. D. (2008). Population imaging of ongoing neuronal activity in the visual cortex of awake rats. *Nature Neuroscience, 11,* 749–751.
Grego, F., Vallier, J.-M., Collardeau, M., Bermon, S., Ferrari, P., Candito, M., et al. (2004). Effects of long duration exercise on cognitive function, blood glucose, and counterregulatory hormones in male cyclists. *Neuroscience Letters, 364,* 76–80.
Gur, M., & Snodderly, D. M. (2007). Direction selectivity in V1 of alert monkeys: Evidence for parallel pathways for motion processing. *Journal of Physiology, 585,* 383–400.
Hottenrott, K., Taubert, M., & Gronwald, T. (2013). Cortical brain activity is influenced by cadence in cyclists. *Open Sports Sciences Journal, 6,* 9–14.
Juni, M. Z., Gureckis, T. M., & Maloney, L. T. (2015). Information sampling behavior with explicit sampling costs. *Decision, 3,* 41.
Keller, G. B., Bonhoeffer, T., & Hübener, M. (2012). Sensorimotor mismatch signals in primary visual cortex of the behaving mouse. *Neuron, 74,* 809–815.
Krauzlis, R. J., Bollimunta, A., Arcizet, F., & Wang, L. (2014). Attention as an effect not a cause. *Trends in Cognitive Sciences, 18,* 457–464.
Laeng, B., Sirois, S., & Gredeback, G. (2012). Pupillometry: A window to the preconscious? *Perspectives on Psychological Science, 7,* 18–27.
Lambourne, K., Audiffren, M., & Tomporowski, P. D. (2010). Effects of acute exercise on sensory and executive processing tasks. *Medicine and Science in Sports and Exercise, 42,* 1396–1402.
Laramée, M.-E., & Boire, D. (2015). Visual cortical areas of the mouse: Comparison of parcellation and network structure with primates. *Frontiers in Neural Circuits, 8,* 149.
Lombardo, M., & Lombardo, G. (2010). Wave aberration of human eyes and new descriptors of image optical quality and visual performance. *Journal of Cataract and Refractive Surgery, 36,* 313–331.
Ludyga, S., Hottenrott, K., & Gronwald, T. (2016). Four weeks of high cadence training alter brain cortical activity in cyclists. *Journal of Sports Sciences, 414,* 1–6.
Maimon, G. (2011). Modulation of visual physiology by behavioral state in monkeys, mice, and flies. *Current Opinion in Neurobiology, 21,* 559–564.
Maimon, G., Straw, A. D., & Dickinson, M. H. (2010). Active flight increases the gain of visual motion processing in Drosophila. *Nature Neuroscience, 13,* 393–399.
McGinley, M. J., David, S. V., & McCormick, D. A. (2015). Cortical membrane potential signature of optimal states for sensory signal detection. *Neuron, 87,* 179–192.
Naselaris, T., Kay, K. N., Nishimoto, S., & Gallant, J. L. (2011). Encoding and decoding in fMRI. *Neuroimage, 56,* 400–410.
Niell, C. M., & Stryker, M. P. (2008). Highly selective receptive fields in mouse visual cortex. *Journal of Neuroscience, 28,* 7520–7536.
Niell, C. M., & Stryker, M. P. (2010). Modulation of visual responses by behavioral state in mouse visual cortex. *Neuron, 65,* 472–479.
Polack, P.-O., Friedman, J., & Golshani, P. (2013). Cellular mechanisms of brain state–dependent gain modulation in visual cortex. *Nature Neuroscience, 16,* 1331–1339.
Pontifex, M. B., & Hillman, C. H. (2007). Neuroelectric and behavioral indices of interference control during acute cycling. *Clinical Neurophysiology, 118,* 570–580.
Ringach, D. L., Bredfeldt, C. E., Shapley, R. M., & Hawken, M. J. (2002). Suppression of neural responses to nonoptimal stimuli correlates with tuning selectivity in macaque V1. *Journal of Neurophysiology, 87,* 1018–1027.
Ringach, D. L., Shapley, R. M., & Hawken, M. J. (2002). Orientation selectivity in macaque V1: Diversity and laminar dependence. *Journal of Neuroscience, 22,* 5639–5651.
Samaha, J., Sprague, T. C., & Postle, B. R. (2016). Decoding and reconstructing the focus of spatial attention from the topology of alpha-band oscillations. *Journal of Cognitive Neuroscience, 28,* 1090–1097.
Saleem, A. B., Ayaz, A., Jeffery, K. J., Harris, K. D., & Carandini, M. (2013). Integration of visual motion and locomotion in mouse visual cortex. *Nature Neuroscience, 16,* 1864–1869.
Sellers, K. K., Bennett, D. V., Hutt, A., Williams, J. H., & Fröhlich, F. (2015). Awake vs. anesthetized: Layer-specific sensory processing in visual cortex and functional connectivity between cortical areas. *Journal of Neurophysiology, 113,* 3798–3815.
Serences, J. T., & Saproo, S. (2012). Computational advances towards linking BOLD and behavior. *Neuropsychologia, 50,* 435–446.
Serences, J. T., Saproo, S., Scolari, M., Ho, T., & Muftuler, L. (2009). Estimating the influence of attention on population codes in human visual cortex using voxel-based tuning functions. *Neuroimage, 44,* 223–231.
Sprague, T. C., Saproo, S., & Serences, J. T. (2015). Visual attention mitigates information loss in small- and large-scale neural codes. *Trends in Cognitive Sciences, 19,* 215–226.
Wilson, A. M., & Glickfeld, L. L. (2014). Visual circuits get the VIP treatment. *Cell, 156,* 1123–1124.
Yerkes, R., & Dodson, J. (1908). The relation of strength of stimulus to rapidity of habit-formation. *Journal of Comparative Neurology and Psychology, 18,* 459–482.
Zénon, A., & Krauzlis, R. J. (2012). Attention deficits without cortical neuronal deficits. *Nature, 489,* 434–437.